

Ly α AND UV SIZES OF GREEN PEA GALAXIESHUAN YANG^{1,2}, SANGEETA MALHOTRA², JAMES E. RHOADS², CLAUS LEITHERER³, AIDA WOFFORD⁴, TIANXING JIANG², JUNXIAN WANG¹*Draft version November 7, 2018*

ABSTRACT

Green Peas are nearby analogs of high-redshift Ly α -emitting galaxies (LAEs). To probe their Ly α escape, we study the spatial profiles of Ly α and UV continuum emission of 24 Green Pea galaxies using the Cosmic Origins Spectrograph (COS) on Hubble Space Telescope (HST). We extract the spatial profiles of Ly α emission from their 2D COS spectra, and of UV continuum from both the 2D spectra and NUV images. The Ly α emission shows more extended spatial profiles than the UV continuum in most Green Peas. The deconvolved Full Width Half Maximum (FWHM) of the Ly α spatial profile is about 2 to 4 times that of the UV continuum in most cases. Since Green Peas are analogs of high- z LAEs, it suggests that most high- z LAEs likely have larger Ly α sizes than UV sizes. We also compare the spatial profiles of Ly α photons at blueshifted and redshifted velocities in eight Green Peas with sufficient data quality, and find the blue wing of the Ly α line has a larger spatial extent than the red wing in four Green Peas with comparatively weak blue Ly α line wings. We show that Green Peas and MUSE $z = 3 - 6$ LAEs have similar Ly α and UV continuum sizes, which probably suggests starbursts in both low- z and high- z LAEs drive similar gas outflows illuminated by Ly α light. Five Lyman continuum (LyC) leakers in this sample have similar Ly α to UV continuum size ratios ($\sim 1.4 - 4.3$) to the other Green Peas, indicating their LyC emission escape through ionized holes in the interstellar medium.

1. INTRODUCTION

The Ly α emission line is a key tool in discovering and studying high redshift galaxies (e.g. Dey et al. 1998; Hu et al. 1998; Rhoads et al. 2000; Ouchi et al. 2003; Matthee et al. 2014; Zheng et al. 2016). At $z > 6$, the Ly α luminosity, Ly α equivalent width (EW), and spatial clustering of Ly α emitting galaxies (LAEs) are important probes of the reionization of Universe (e.g. Malhotra & Rhoads 2004; Kashikawa et al. 2011; Treu et al. 2012; Pentericci et al. 2014; Tilvi et al. 2014). To understand LAEs and reionization requires us to understand how Ly α escape from galaxies.

Since Ly α is a resonant line, the Ly α escape depends on the amount of dust, the HI gas column density (N_{HI}), the velocity distribution of HI gas, and the geometric distribution of HI gas and dust (e.g. Neufeld 1990; Charlott & Fall 1993; Verhamme et al. 2006; Dijkstra et al. 2006). One important indicator of Ly α escape processes is the Ly α spatial distribution. The Ly α emission would be confined to HII regions and have similar size to the UV continuum emission if most Ly α photons escape from ionized holes in the interstellar medium (ISM). Instead, if most Ly α photons diffuse out of galaxy through numerous resonant scatterings, the Ly α emission would be more extended than the UV continuum (e.g. Östlin et al. 2009; Zheng et al. 2010; Hayes et al. 2014).

Prior HST studies of Ly α morphology in low redshift starburst galaxies usually show diffuse Ly α emission in

the outer part of galaxy and sometimes Ly α absorption in the center of galaxy (Kunth et al. 2003; Mas-Hesse et al. 2003; Östlin et al. 2009, Hayes et al. 2005, 2014). But most of those low redshift starbursts have much lower Ly α EW ($EW < 20 \text{ \AA}$) and Ly α escape fraction ($f_{\text{esc}}^{\text{Ly}\alpha}$) than high- z LAEs. Since Ly α photons escape more easily and probably have fewer scatterings in high- z LAEs, it is reasonable to suppose that LAEs with high Ly α EW may have compact Ly α sizes. Due to the faintness of high- z LAEs, there are only two studies of Ly α size with high resolution HST narrow-band imaging for a few high- z LAEs (Bond et al. 2010; Finkelstein et al. 2011), and they reached contradictory conclusions: Bond et al. (2010) suggested Ly α sizes are compact and similar to UV continuum emission; but Finkelstein et al. (2011) suggested Ly α appears larger than the UV continuum.

Many ground based studies of Ly α morphology suggest that a large scale faint Ly α halo is common in high- z Ly α galaxies due to the scatterings of Ly α photons by the HI gas in circum-galactic medium (e.g. Moller & Warren 1998; Swinbank et al. 2007; Rauch et al. 2008; Steidel et al. 2011; Mastuda et al. 2012; Feldmeier et al. 2013; Momose et al. 2015; Wisotzki et al. 2015; Matthee et al. 2016). As the ground based data has low spatial resolution, however, it is still unclear if the Ly α morphology of LAEs on galactic scales is compact or larger than the UV continuum, and if they show central Ly α absorption.

Green Pea galaxies are compact starburst galaxies with strong [OIII] λ 5007 emission lines ($EW([\text{OIII}]\lambda 5007) > 300 \text{ \AA}$) in the nearby universe (Cardamone et al. 2009). They have strong Ly α emission lines (Jaskot et al. 2014; Henry et al. 2015; Yang et al. 2016); and their Ly α EW distribution is similar to high- z LAEs (Yang et al. 2016). Five Green Peas in our sample also show Lyman contin-

¹ CAS Key Laboratory for Research in Galaxies and Cosmology, Department of Astronomy, University of Science and Technology of China; huan.y@asu.edu

² Arizona State University, School of Earth and Space Exploration

³ Space Telescope Science Institute

⁴ National Autonomous University of Mexico, Institute of Astronomy

uum emission (Izotov et al. 2016). In this paper, we study the spatial distribution of Ly α and UV emission of 24 Green Peas with HST-COS, compare the spatial profiles of Ly α photons at blue and red velocities, and discuss the implications to Ly α and LyC escape.

2. OBSERVATIONS AND DATA ANALYSIS

In Yang et al. (2017), we assemble a sample of 43 Green Peas with HST-COS spectroscopic observations. Comparing to the parent sample of Green Peas in Cardamone et al. (2009), this sample covers the full ranges of properties, such as dust extinction, metallicity, and star formation rate (figure 1 in Yang et al. 2017). Thus it is a representative sample of Green Peas. From this sample, we select 24 Green Peas which have good spatial resolution (Full Width at Half Maximum, FWHM $\sim 0.3 - 0.4''$ for point source) in their 2D spectra. Since the COS FUV channel is not corrected for spherical aberration, the cross-dispersion resolution of COS FUV spectra depends on the chosen grating, the wavelength position (WP) of the grating, and the wavelength (COS ISR2013_07). The grating and WP are chosen based on considerations of wavelength coverages and the gap in FUV detectors, thus varies mostly with the redshifts. Although this sample only covers a small redshift range ($\sim 0.1 - 0.3$), a slightly different redshift, thus a different grating WP, can result in very different spatial resolution in the 2D spectra. So these 24 selected Green Peas are not statistically different from the sample of 43 Green Peas in obvious ways.

High resolution NUV acquisition images were taken with the COS acquisition mode ACS/IMAGE for all 24 Green Peas. Their FUV spectra were taken with the $2.5''$ diameter Primary Science Aperture and the G160M grating, which has the best spatial resolution in all COS gratings.

The COS FUV grating G160M has five WP – 1577Å, 1589Å, 1600Å, 1611Å, 1623Å. The WP=1623Å has the best spatial resolution and 15/24 of Green Peas are taken in this WP. The COS spatial resolutions are about $0.3 - 0.4''$ for point source and stable with wavelength for the WP=1600Å, 1611Å, and 1623Å, but are larger and vary moderately with wavelength for the WP=1577Å and 1589Å. We generally avoid using objects with WP=1577Å or 1589Å except for three cases where their Ly α emission lines are in wavelength ranges with small spatial resolution. The WP of each object is shown in Table 1.

We retrieved COS spectra of these 24 Green Peas from the HST MAST archive after they have been processed through the standard COS pipeline. The calibrated two dimensional Ly α and FUV spectra are shown in figure 1. We extract the spatial profiles of Ly α along the sky direction by summing the spectra in a wavelength range about 1211–1220 Å along the dispersion direction. We extract the spatial profiles of FUV continuum in wide wavelength ranges of a few tens Angstroms near Ly α lines in the same spectra segment. Then we sum the spatial profiles from spectra taken at different central wavelengths or FP-POS settings for each Green Pea. In figure 2, we show their normalized spatial profiles of Ly α and FUV continuum light. The pixel scale along the sky direction is $0.1''/\text{pixel}$. Since the COS FUV detector counts photons, we assume the photon counts in each

spatial bin follows Poisson statistics, and calculate its statistical error as $\text{counts}_{\text{err}} = (\text{counts})^{1/2}$.

In figure 2, we also show the instrumental spatial profile of each object derived from observations of a point source in the same grating and WP (WD1057+719, CAL/COS 12806, PI: Derck Massa). Since the spatial resolution slightly varies with wavelength, the instrumental profiles are extracted for Ly α and FUV continuum separately in the corresponding wavelength ranges that are used to extract the Ly α and FUV spectra of each object.

The response of COS/FUV detector decreases with usage, a process called gain-sag. To mitigate these gain-sag effects, COS/FUV spectra are moved to pristine locations of the detector, i.e. different lifetime positions (LP) every 2-3 years. Our sample spans on all three lifetime positions (LP1, LP2, and LP3). As we only use the data with small spatial resolution, the spatial profiles are separated from the insensitive detector regions of earlier LPs. The LP of each object is shown in Table 1.

We then measure the Ly α EW and Ly α escape fraction ($f_{\text{esc}}^{\text{Ly}\alpha}$) of this sample (details in Yang et al. 2016b). The $f_{\text{esc}}^{\text{Ly}\alpha}$ is defined as the ratio of the measured Ly α flux to intrinsic Ly α flux. Assuming case-B recombination, the intrinsic Ly α flux is about 8.7 times dust extinction corrected H α flux measured from SDSS spectra. Thus the $f_{\text{esc}}^{\text{Ly}\alpha}$ is $\text{Ly}\alpha(\text{observed})/(8.7 \times \text{H}\alpha_{\text{corrected}})$. In Table 1, we show their redshifts, Ly α equivalent widths, and Ly α escape fractions.

3. COMPARE SPATIAL PROFILES OF Ly α AND UV EMISSION

From the 2D spectra and 1D spatial profiles, we can see that the Ly α emission comes from a larger region than the FUV emission in most of these 24 Green Peas. The spatial profiles of UV are only slightly larger than the instrumental profiles, but the spatial profiles of Ly α are well resolved and show asymmetric spatial distributions in many cases. In four cases with low $f_{\text{esc}}^{\text{Ly}\alpha}$ (GP1457+2232, GP0303–0759, GP0752+1638, and GP1244+0216), Ly α light shows a significant offset from the FUV continuum (similar to some high- z LAEs in Micheva et al. 2015). In GP1429+0643, a large fraction of the Ly α emission in the galactic center is absorbed, resulting in a double horned spatial profile.

To characterize the size of spatial profile, we measure the FWHM (FWHM $_m$) of each profile. The FWHM is not sensitive to the depth of the observation. To get the error of FWHM $_m$ of each observed spatial profile, we simulate 1000 fake profiles by adding random Gaussian errors to the observed profile. We measure the FWHM $_m$ of each fake profile and calculate the standard deviation of the 1000 fake profiles as the error of FWHM $_m$ for each observed spatial profile. The measured FWHM $_m$ and its errors are shown in Table 2. We can see again that the Ly α emission have significantly larger FWHM $_m$ than the UV continuum emission.

3.1. The Deconvolved Sizes of Ly α and UV emission

To estimate the deconvolved sizes, we assume the intrinsic Ly α or UV emission follows an exponential profile with scale radius r_e and convolve the exponential profile with the instrumental profile, so we get a relation between observed FWHM and intrinsic FWHM. Since

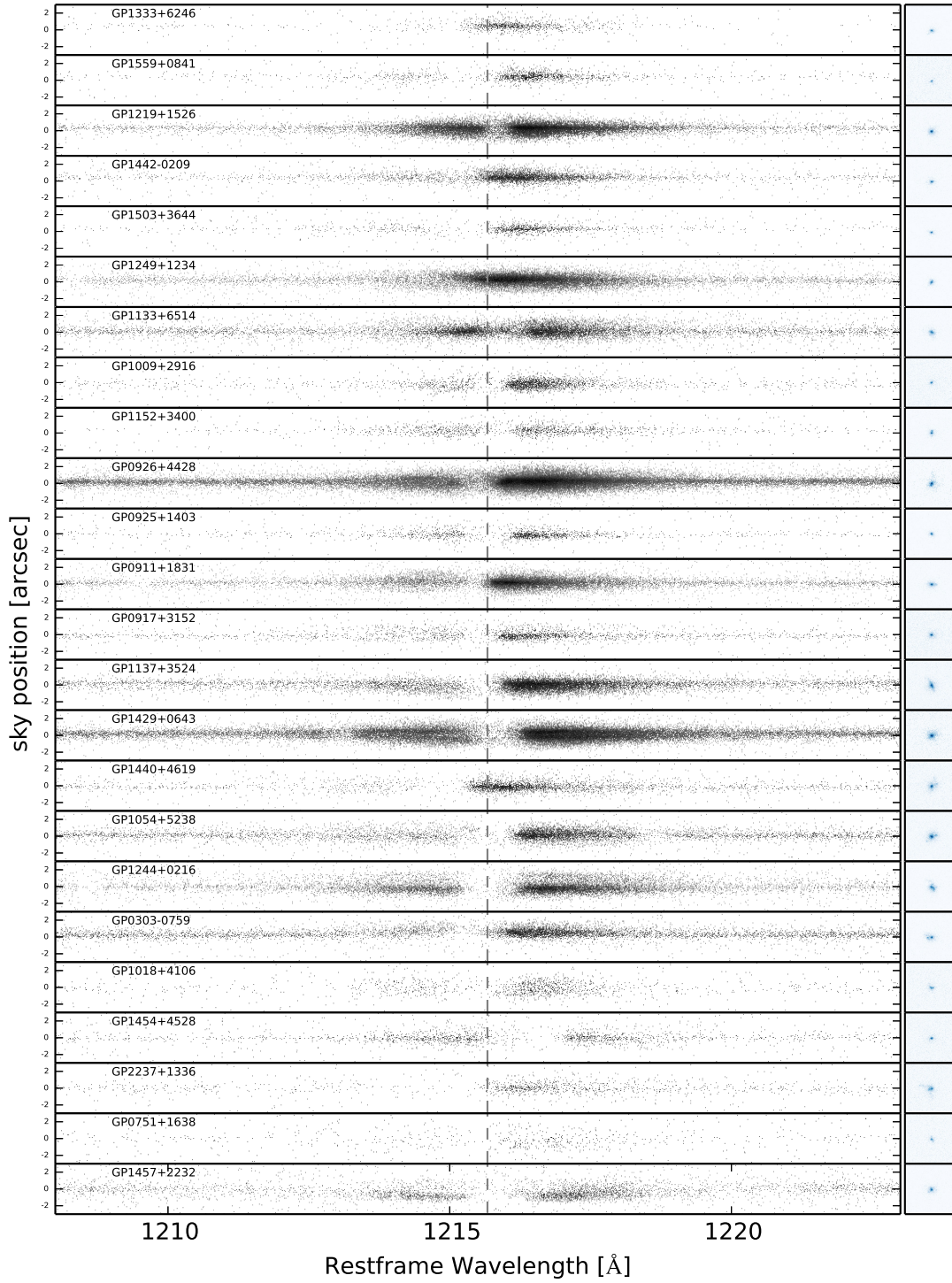


FIG. 1.— The 2D FUV spectra and NUV images of these 24 Green Peas. In the 2D spectra, X axis is along the dispersion direction and Y axis is along the sky direction. The COS aperture is a 2.5 arc-second diameter circle. The dashed vertical line marks the restframe wavelength of Ly α . The NUV images ($6'' \times 6''$) are at the same orientation as the 2D spectra. All NUV images have the same range of color-bar in log-scale. These 24 galaxies are sorted by decreasing $f_{esc}^{Ly\alpha}$ from top to bottom. The ID of each galaxy is marked in each panel.

the throughput begins to decrease when the offset from aperture center is larger than about $0.5''$, we multiply

the convolved profile with a throughput curve of G160M retrieved from COS instrumental handbook. In figure 3,

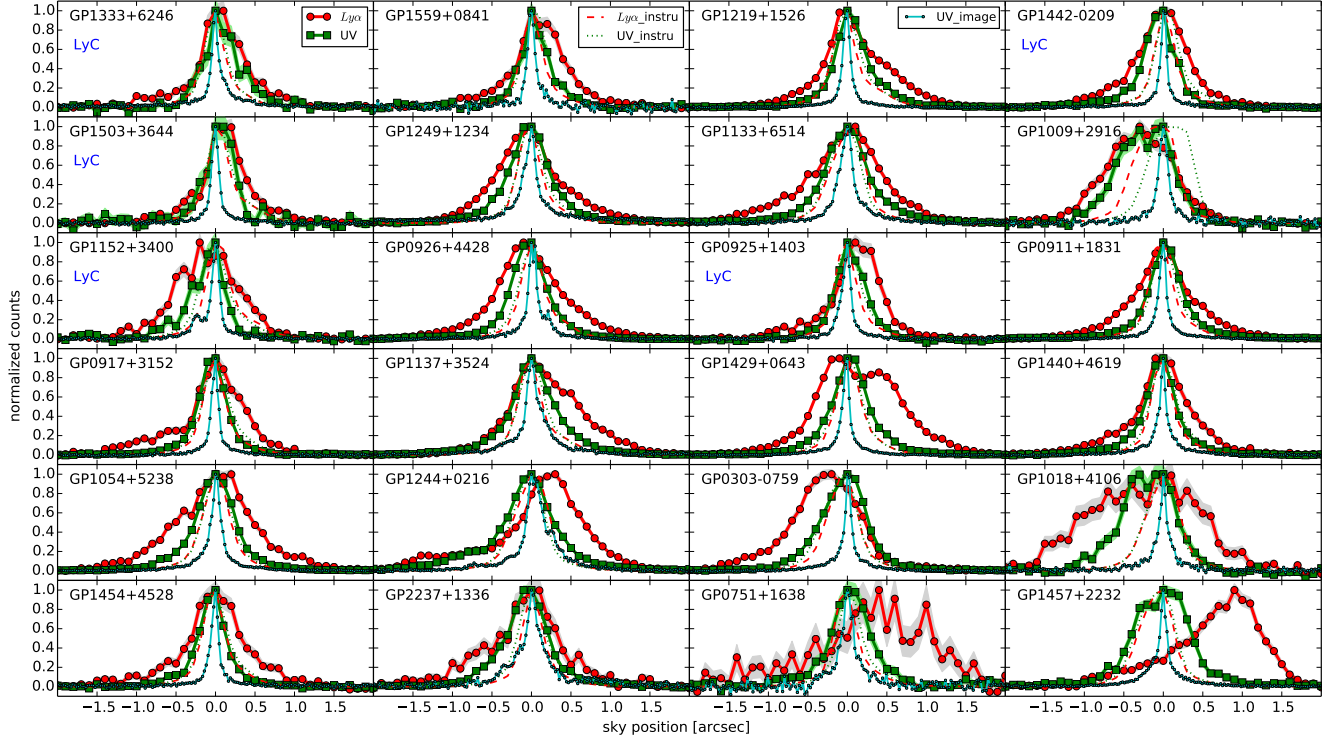


FIG. 2.— The normalized spatial profiles along the sky direction for the 24 Green Peas. In each panel, the solid green line with square marker shows the spatial profiles of the UV continuum emission measured from COS, and the solid red line with circle marker shows the spatial profiles of total Ly α emission. The shaded grey (light-green) regions of the solid red (green) lines show the 1σ errors of the Ly α (UV) spatial profiles. The dotted green and dashed red lines show the instrumental spatial profiles for UV continuum and Ly α emission respectively. The instrumental spatial profiles are derived from observations of a white dwarf point source (Section 2). The solid cyan line with dot marker shows the spatial profiles of UV continuum emission measured from NUV acquisition image along the spatial direction of 2D spectra. These 24 galaxies are sorted by decreasing $f_{esc}^{Ly\alpha}$ from top to bottom and from left to right. Five LyC leakers in this sample (Izotov et al. 2016) are marked with “LyC”.

we show an example of the profile convolution and how the FWHM of convolved profile varies with the r_e of intrinsic profile. We then calculate the deconvolved size of Ly α emission as the FWHM of the exponential profile which has the same FWHM $_m$ as the observed Ly α spatial profile. Since the measured FWHM $_m$ of Ly α emission (about $0.6'' - 1.0''$) are within the angular ranges with $\gtrsim 80\%$ throughput, the Ly α sizes are *not* underestimated due to attenuation at large offsets except in GP1018+4106 which has very large Ly α size.

Since the NUV image has a spatial resolution of about $0.04''$ (less than 2 pixels at pixels scale of $0.0235''/\text{pixel}$), the NUV emission of this sample are well resolved. We estimate the NUV size from the NUV acquisition image shown in figure 1 at the same orientation as the 2D spectra. We extract spatial profiles by summing the pixels in the image along the dispersion direction. Then we calculate the intrinsic NUV sizes as the FWHM of the NUV spatial profiles. The results are shown in Table 2.

Ideally, the deconvolved FUV size and NUV size should be similar. However, when the observed FUV profile and instrumental profile are very similar, the deconvolution failed and resulted in very small deconvolved FUV size. To compare the sizes of Ly α and UV emission, we use the larger one of $FWHM_d(FUV)$ and $FWHM(NUV)$, so we get a conservative Ly α to UV size ratio. The deconvolved Ly α sizes are typically 2.6 times of the UV sizes and vary between 1.4 and 4.3 times for 22 out of

the 24 Green Peas. In GP1429+0643 which has a double horned spatial profile, the deconvolved Ly α FWHM is about 7 times the UV FWHM. In GP1018+4106, the deconvolved Ly α FWHM is badly constrained and can be 3.5 – 13 times larger than the UV FWHM.

4. COMPARING SPATIAL PROFILES OF Ly α PHOTONS AT DIFFERENT VELOCITIES

Green Peas usually show double-peaked Ly α velocity profiles (Jaskot et al. 2014; Henry et al. 2015; Yang et al. 2016). The Ly α photons with different velocities are scattered differently by the HI gas. Since we have the 2D Ly α spectra, we can compare the spatial profiles of Ly α photons at different velocities. We define the blue-part (red-part) as the negative-velocity-side (positive-velocity-side) of the inter-peak dip of the Ly α velocity profile. For one object (GP1249+1234) with a single peaked Ly α velocity profile, we separate the blue-part and red-part by velocity=0. Then we extract the spatial profiles of the blue-part and red-part Ly α emission. Since the blue-part is usually weaker than the red-part Ly α emission, we show the 8 of 24 Green Peas with the best signal-to-noise ratio in the blue-part Ly α emission. These 8 Green Peas also have relatively high $f_{esc}^{Ly\alpha}$. We compare their spatial profiles of blue-part and red-part Ly α emission in figure 4.

The spatial profiles of blue-part and red-part Ly α emission are generally similar. But in four cases (GP1137+3524, GP1249+1234, GP0911+1831, and

TABLE 1

ID	RA	DEC	Redshift	EW(Ly α)	$f_{esc}^{Ly\alpha}$	WP	LP#	GO#
(1)	(2)	(3)	(4)	(5)	(6)	(7)	(8)	(9)
GP1333+6246 ^a	13:33:03.94	+62:46:03.7	0.318124	65.3	1.066	1623	3	13744
GP1559+0841	15:59:25.98	+08:41:19.1	0.297036	89.0	0.682	1623	3	14201
GP1219+1526	12:19:03.98	+15:26:08.5	0.195599	157.5	0.672	1623	2	12928
GP1442+0209 ^a	14:42:31.37	+02:09:52.8	0.293669	127.9	0.408	1623	3	13744
GP1503+3644 ^a	15:03:42.82	+36:44:50.8	0.355689	99.6	0.402	1623	3	13744
GP1249+1234	12:48:34.64	+12:34:02.9	0.263389	94.8	0.384	1623	2	12928
GP1133+6514	11:33:03.80	+65:13:41.3	0.241397	35.3	0.352	1600	2	12928
GP1009+2916	10:09:18.99	+29:16:21.5	0.221918	62.5	0.335	1589	3	14201
GP1152+3400 ^a	11:52:04.88	+34:00:49.9	0.341946	67.5	0.260	1623	3	13744
GP0926+4428	09:26:00.44	+44:27:36.5	0.180690	40.8	0.245	1611	1	11727
GP0925+1403 ^a	09:25:32.37	+14:03:13.1	0.301211	83.0	0.171	1623	3	13744
GP0911+1831	09:11:13.34	+18:31:08.2	0.262200	49.5	0.155	1623	2	12928
GP0917+3152	09:17:02.52	+31:52:20.6	0.300364	31.0	0.138	1623	3	14201
GP1137+3524	11:37:22.14	+35:24:26.7	0.194390	33.4	0.130	1623	2	12928
GP1429+0643	14:29:47.03	+06:43:34.9	0.173509	35.7	0.103	1600	2	13017
GP1440+4619	14:40:09.94	+46:19:36.9	0.300758	26.8	0.101	1623	3	14201
GP1054+5238	10:53:30.83	+52:37:52.9	0.252638	10.7	0.068	1611	2	12928
GP1244+0216	12:44:23.37	+02:15:40.4	0.239426	40.0	0.065	1600	2	12928
GP0303+0759	03:03:21.41	+07:59:23.2	0.164880	7.2	0.050	1589	2	12928
GP1018+4106	10:18:03.24	+41:06:21.1	0.237052	26.1	0.047	1600	3	14201
GP1454+4528	14:54:35.58	+45:28:56.3	0.268505	23.0	0.047	1623	3	14201
GP2237+1336	22:37:35.06	+13:36:47.0	0.293501	9.9	0.034	1623	3	14201
GP0751+1638	07:51:57.80	+16:38:13.2	0.264713	8.8	0.024	1623	3	14201
GP1457+2232	14:57:35.13	+22:32:01.8	0.148611	5.3	0.010	1577	2	13293

NOTE. — Column descriptions: (5-6) restframe Ly α equivalent width, and Ly α escape fraction from Yang et al. (2016b, in-prep); (7) Central wavelength position of G160M grating; (8) COS lifetime position (LP); (9) HST programs: GO14201 (PI S. Malhotra), GO13744 (PI T. Thuan; Izotov et al. 2016), GO13293 (PI A. Jaskot; Jaskot et al. 2014), GO12928 (PI A. Henry; Henry et al. 2015), GO11727 and GO13017 (PI T. Heckman; Heckman et al. 2011; Alexandroff et al. 2015).

^a These are confirmed LyC leakers from Izotov et al. (2016).

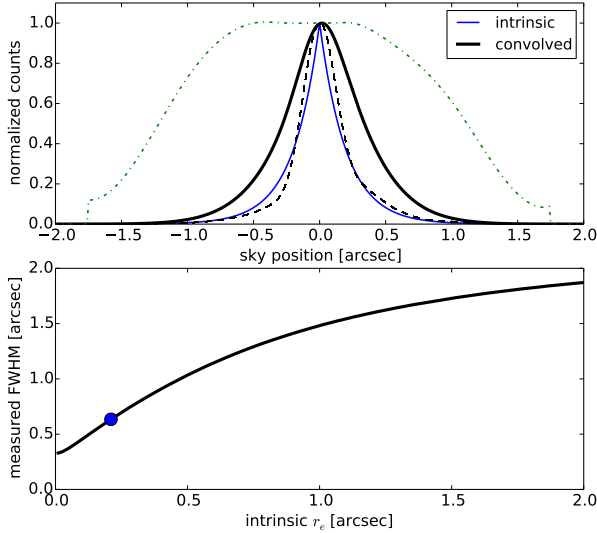


FIG. 3.— Top panel: an example of the profile convolution. The dashed black line is a typical instrumental profile for Ly α emission. The thin solid blue line shows the intrinsic spatial profile of Ly α emission which is assumed to be an exponential profile (a typical profile with $r_e = 0.2''$ is shown). The thick solid black line is the convolved profile after convolving the intrinsic profile with the instrumental profile and multiplying it by the throughput profile (dash-dotted green line). Bottom panel: the measured FWHM of the convolved profile as a function of the r_e of the intrinsic profile. The blue point shows a typical value of the intrinsic Ly α size in our sample.

GP0926+4428), the blue-part Ly α emission are more extended than the red-part Ly α emission. In the other four

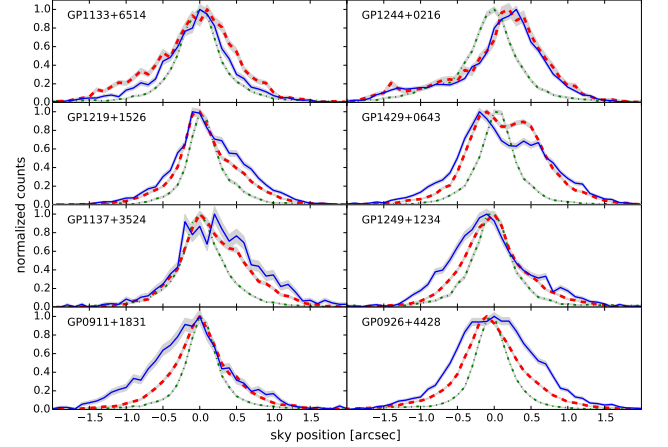


FIG. 4.— Comparison between the spatial profiles of the blueshifted and redshifted portions of the Ly α emission lines for 8 objects with the best signal-to-noise ratio in the blue-part Ly α emission. Since the Ly α velocity profiles are usually double-peaked, we define the blue-part (red-part) as the negative-velocity-side (positive-velocity-side) of the inter-peak dip of the Ly α velocity profile. The solid blue lines, dashed red lines, and dotted green lines show the spatial profiles of blue-part Ly α , red-part Ly α , and UV continuum emission correspondingly. The shaded grey regions of lines show the 1σ errors of the spatial profiles.

cases (GP1244+0216, GP1133+6514, GP1429+0643, and GP1219+1526), the blue-part and red-part Ly α emission are very similar. We also noticed that the Ly α spatial profiles show a relation with the Ly α velocity profiles – the objects with weaker blue peak in Ly α velocity profile (i.e. small flux ratio of blue-part to red-part Ly α emission), such as GP1137+3524, GP0911+1831, and GP0926+4428, also have broader blue-part spatial

TABLE 2

ID	FWHM _m (Ly α)	FWHM _m (FUV)	FWHM _d (Ly α)	FWHM _d (FUV)	FWHM(NUV)	$\frac{FWHM(Ly\alpha)}{FWHM(UV)}$
(1)	arcsec (2)	arcsec (3)	arcsec (4)	arcsec (5)	arcsec (6)	(7)
GP1333+6246 ^a	0.56 \pm 0.04	0.38 \pm 0.08	0.24 $^{+0.04}_{-0.03}$	0.08 $^{+0.07}_{-0.07}$	0.09	2.62 $^{+0.80}_{-0.52}$
GP1559+0841	0.56 \pm 0.04	0.35 \pm 0.04	0.25 $^{+0.04}_{-0.04}$	0.04 $^{+0.04}_{-0.03}$	0.11	2.27 $^{+0.67}_{-0.55}$
GP1219+1526	0.65 \pm 0.03	0.42 \pm 0.01	0.29 $^{+0.01}_{-0.03}$	0.06 $^{+0.01}_{-0.01}$	0.11	2.65 $^{+0.43}_{-0.47}$
GP1442-0209 ^a	0.70 \pm 0.04	0.44 \pm 0.03	0.37 $^{+0.04}_{-0.04}$	0.12 $^{+0.03}_{-0.03}$	0.08	3.00 $^{+1.29}_{-0.82}$
GP1503+3644 ^a	0.48 \pm 0.04	0.38 \pm 0.06	0.15 $^{+0.03}_{-0.03}$	0.06 $^{+0.06}_{-0.04}$	0.11	1.39 $^{+0.43}_{-0.36}$
GP1249+1234	0.75 \pm 0.02	0.56 \pm 0.02	0.39 $^{+0.03}_{-0.01}$	0.19 $^{+0.01}_{-0.01}$	0.17	2.00 $^{+0.31}_{-0.20}$
GP1133+6514	0.96 \pm 0.06	0.58 \pm 0.01	0.54 $^{+0.07}_{-0.07}$	0.17 $^{+0.01}_{-0.01}$	0.20	2.70 $^{+0.69}_{-0.56}$
GP1009+2916	0.95 \pm 0.06	0.82 \pm 0.04	0.46 $^{+0.07}_{-0.07}$	0.30 $^{+0.06}_{-0.06}$	0.14	1.50 $^{+0.61}_{-0.42}$
GP1152+3400 ^a	0.87 \pm 0.09	0.44 \pm 0.07	0.47 $^{+0.08}_{-0.10}$	0.08 $^{+0.06}_{-0.07}$	0.11	4.28 $^{+1.32}_{-1.19}$
GP0926+4428	0.82 \pm 0.01	0.49 \pm 0.01	0.44 $^{+0.01}_{-0.01}$	0.14 $^{+0.01}_{-0.01}$	0.12	3.20 $^{+0.47}_{-0.38}$
GP0925+1403 ^a	0.58 \pm 0.04	0.42 \pm 0.03	0.26 $^{+0.03}_{-0.03}$	0.08 $^{+0.01}_{-0.03}$	0.12	2.19 $^{+0.50}_{-0.41}$
GP0911+1831	0.62 \pm 0.02	0.44 \pm 0.01	0.28 $^{+0.03}_{-0.01}$	0.11 $^{+0.01}_{-0.01}$	0.10	2.50 $^{+0.64}_{-0.39}$
GP0917+3152	0.62 \pm 0.04	0.39 \pm 0.01	0.30 $^{+0.04}_{-0.04}$	0.04 $^{+0.01}_{-0.03}$	0.10	3.05 $^{+0.80}_{-0.66}$
GP1137+3524	0.88 \pm 0.02	0.56 \pm 0.01	0.49 $^{+0.03}_{-0.01}$	0.19 $^{+0.01}_{-0.01}$	0.18	2.50 $^{+0.35}_{-0.23}$
GP1429+0643	1.18 \pm 0.02	0.49 \pm 0.01	0.90 $^{+0.01}_{-0.07}$	0.12 $^{+0.01}_{-0.01}$	0.09	7.22 $^{+1.03}_{-1.22}$
GP1440+4619	0.62 \pm 0.04	0.42 \pm 0.01	0.29 $^{+0.04}_{-0.03}$	0.07 $^{+0.01}_{-0.01}$	0.08	3.64 $^{+0.98}_{-0.65}$
GP1054+5238	0.99 \pm 0.07	0.54 \pm 0.01	0.62 $^{+0.10}_{-0.08}$	0.17 $^{+0.01}_{-0.01}$	0.13	3.75 $^{+0.98}_{-0.75}$
GP1244+0216	0.82 \pm 0.03	0.63 \pm 0.02	0.39 $^{+0.04}_{-0.03}$	0.22 $^{+0.01}_{-0.03}$	0.24	1.62 $^{+0.37}_{-0.25}$
GP0303-0759	0.94 \pm 0.04	0.63 \pm 0.02	0.55 $^{+0.04}_{-0.04}$	0.19 $^{+0.01}_{-0.01}$	0.08	2.86 $^{+0.45}_{-0.39}$
GP1018+4106	1.75 \pm 0.27	0.76 \pm 0.04	2.15 $^{+1.80}_{-0.83}$	0.33 $^{+0.04}_{-0.03}$	0.10	6.46 $^{+6.50}_{-2.94}$
GP1454+4528	0.62 \pm 0.05	0.37 \pm 0.02	0.29 $^{+0.04}_{-0.06}$	0.01 $^{+0.04}_{-0.01}$	0.10	2.91 $^{+0.79}_{-0.77}$
GP2237+1336	0.68 \pm 0.11	0.56 \pm 0.03	0.36 $^{+0.10}_{-0.11}$	0.18 $^{+0.03}_{-0.01}$	0.20	1.80 $^{+0.74}_{-0.67}$
GP0751+1638	0.97 \pm 0.32	0.53 \pm 0.04	0.62 $^{+0.42}_{-0.32}$	0.19 $^{+0.04}_{-0.03}$	0.17	3.21 $^{+3.04}_{-1.92}$
GP1457+2232	0.92 \pm 0.09	0.80 \pm 0.03	0.50 $^{+0.10}_{-0.10}$	0.33 $^{+0.04}_{-0.03}$	0.10	1.50 $^{+0.45}_{-0.43}$

NOTE. — Column descriptions: (2-3) measured Full Width Half Maximum (FWHM) of Ly α and UV spatial profiles. (4-5) $FWHM_d(Ly\alpha)$ and $FWHM_d(FUV)$ are deconvolved FWHM of Ly α and UV derived by mapping measured FWHM to intrinsic values (see section 3.1 and figure 3). (6) FWHM of 1D NUV profile. We convert the 2D NUV images into a 1D profile along the sky direction of spectra. (7) Ratios of $FWHM(Ly\alpha)$ to $FWHM(UV)$. When calculating the ratio, we use the larger one of $FWHM_d(FUV)$ and $FWHM(NUV)$. These 24 galaxies are sorted by decreasing $f_{esc}^{Ly\alpha}$ from top to bottom.

^a These are confirmed LyC leakers from Izotov et al. (2016).

profiles. On the other hand, GP1133+6514, which has the strongest blue peak in Ly α velocity profile, seems to show slightly more compact blue-part Ly α emission than the red-part Ly α emission.

In four Green Peas (GP1219+1526, GP1133+6514, GP0926+4428, and GP1429+0643), the Ly α velocity profiles show large residual emission at velocity near zero. From their 2D spectra (figure 1), we find that the Ly α emission at velocity near zero seems to have more extended Ly α emission than the Ly α emission at other velocities.

Since the outflowing HI gas presented in many Green Peas has larger optical depth to the blue-part Ly α photons than to the red-part Ly α photons, we expect that the escaped blue-part Ly α photons went through more scatterings on average and were scattered to larger radius. For the Ly α photons at velocity near zero, the optical depth is the largest and their spatial profiles also show the largest sizes.

5. DISCUSSION

5.1. Comparison to Previous Results

Many studies measured the Ly α morphology of some nearby star-forming galaxies with HST/STIS (Mas-Hesse et al. 2003) and HST/ACS images (e.g. Kunth et al. 2003, Hayes et al. 2005; Östlin et al. 2009, 2014). Mas-

Hesse et al. (2003) analyzed the HST/STIS 2D spectra of Ly α and UV emission and showed that both Haro 2 and IRAS 0833+6517 have low Ly α EW (6 Å and 12 Å) and larger Ly α sizes than UV continuum sizes, and that their Ly α peaks are offset from the peaks of UV continuum emission.

The LARS program studies the Ly α morphology of 14 nearby starburst galaxies (Hayes et al. 2014; Östlin et al. 2014). 9 out of the 14 galaxies have low Ly α EW and escape fraction and they also show Ly α absorption or weak Ly α emission in the central part of galaxy and diffuse Ly α emission in the outer part of the galaxy. The other 5 galaxies (LARS01, 02, 05, 07, and 14, LARS14 is the same galaxy GP0926+4428 in our sample) are LAEs with relatively high Ly α EW and are comparable to most of the Green Peas in our sample. These five galaxies also have [OIII] λ 5007 equivalent width about 200–300 Å in their SDSS spectra. The Ly α emission in LARS01 shows an offset from the UV emission, and is very similar to the four cases with Ly α -UV offsets in our sample. The Ly α emission in LARS05 shows partial central absorption and is very similar to GP1429+0643, the double-horned case in our sample. The 20% Petrosian radius of Ly α emission of these five galaxies are 2.3 – 3.6 times larger than the 20% Petrosian radius of H α emission (Hayes et al. 2014), which are very similar to the Ly α /UV FWHM ratios in

our sample.

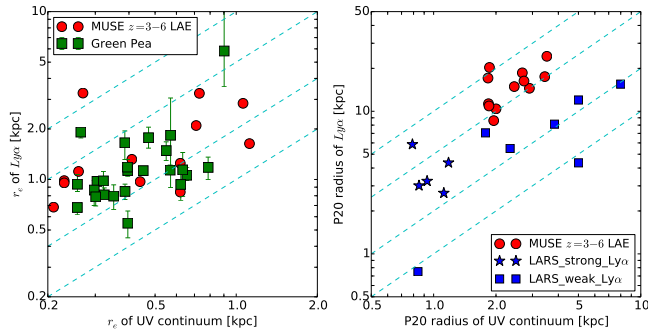


FIG. 5.— Left: Comparison of the Ly α to UV scale length of Green Peas (green squares) and MUSE $z = 3 - 6$ LAEs sample (red dots) (Wisotzki et al. 2016). The Ly α scale lengths of MUSE LAEs are measured from the radial profile in Wisotzki et al. (2016) using the same method as Green Peas. Right: Comparison of the Ly α to UV Petrosian 20% (P20) radius of LARS ~ 0 galaxies and MUSE LAEs. Notice that the Petrosian 20% radius of MUSE sample is measured from the best fit model of radial profile. The dashed cyan lines show constant ratios of 1:1, 2:1, 5:1, and 10:1.

Two studies measure Ly α sizes of 5 high- z LAEs with high resolution HST narrow-band imaging (Bond et al. 2010; Finkelstein et al. 2011). Bond et al. (2010) suggested Ly α sizes are compact and similar to UV emission; but Finkelstein et al. (2011) suggested the half light radius of Ly α appears ~ 1.6 times larger than the half light radius of UV continuum. These narrow band HST images of high- z LAEs are very hard to get and have low S/N ratios, thus the Ly α and UV sizes of low- z LAEs are valuable. Since Green Peas are analogs of high- z LAEs, our results suggest that most high- z LAEs likely have larger Ly α sizes than UV sizes. The extended Ly α emission probably indicates gas outflows around galaxies illuminated by Ly α light.

One interesting question regards the redshift evolution of Ly α sizes of LAEs. Recently, Wisotzki et al. (2016) measured Ly α radial profiles of a sample of LAEs at $z = 3 - 6$ from VLT/MUSE data and found that in 12 LAEs with both Ly α and UV continuum sizes, the Ly α light is considerably more extended than the UV continuum light. Here we compare the sizes of Green Peas and the MUSE LAEs. Using the Ly α radial profiles in Wisotzki et al. (2016), we measured the deconvolved Ly α scale radius r_e assuming an intrinsic exponential profiles, so that the methods are same when measuring the r_e of MUSE LAEs and Green Peas. As shown in figure 5, the Ly α to UV sizes ratios of Green Peas and MUSE LAEs are very similar. (Notice that some MUSE LAEs have extended Ly α halos far beyond the scale radius. But for Green Peas, we don't have robust data to characterize the Ly α emission beyond a few Kpcs.)

In the right panel of figure 5, we compare the Petrosian 20% radius (R_{P20}) of MUSE LAEs (Table 2 in Wisotzki et al. (2016)) to that of the LARS sample (Table 1 in Hayes et al. (2013)). Compared to the five strong Ly α emitters in LARS sample (marked by stars, LARS01, 02, 05, 07, and 14), the MUSE LAEs only have about 2 times larger ratios of $R_{P20}(\text{Ly}\alpha)$ to $R_{P20}(\text{UV})$. One caveat of the comparison is that the Petrosian radius of MUSE sample is measured from the best fit *model*

of radial profile, instead of the observed data, which is different from the method used in LARS sample. This might be the reason that the $R_{P20}(\text{UV})$ of MUSE LAEs are about 2 – 4 kpc, about a factor of three larger than the $R_{P20}(\text{UV})$ of the five LARS Ly α emitters.

Based on our rough comparison of Green Peas and MUSE LAEs, the scale lengths of Ly α and UV continuum have small evolution with redshift. This is not surprising considering that Green Peas and high- z LAEs have very similar galactic properties such as stellar mass, star formation rate, and starburst age. The starburst in Green Peas and LAEs can drive gas outflows to the outer part of galaxies, and the gas outflows can scatter the Ly α light and make the extended Ly α emission.

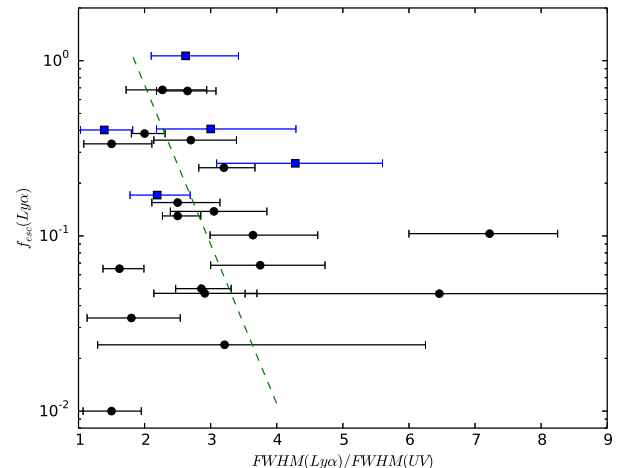


FIG. 6.— The relation between $f_{esc}^{\text{Ly}\alpha}$ and the size ratio $\text{FWHM}(\text{Ly}\alpha)/\text{FWHM}(\text{UV})$ (column (7) of Table 2). The blue square shows the five LyC leakers in this sample. The dashed green line shows a linear fit to the points with $f_{esc}^{\text{Ly}\alpha} > 0.1$. The Spearman correlation coefficient for the points with $f_{esc}^{\text{Ly}\alpha} > 0.1$ is $r = -0.41$ with null probability = 0.11.

5.2. Implication for Ly α and LyC Escape

Our results indicate Ly α have larger sizes than the UV continuum. Since Ly α is a resonant line, our results suggest most Ly α photons escape out of galaxy through many resonant scatterings in the low HI column density gas in Green Peas. If there are fewer scatterings in the Ly α escape process, the Ly α escape fraction would be higher and the Ly α emission would be more compact. So there may be an anti-correlation between $f_{esc}^{\text{Ly}\alpha}$ and the size of Ly α light. In figure 6, we show the relation between $f_{esc}^{\text{Ly}\alpha}$ and the size ratio $\text{FWHM}(\text{Ly}\alpha)/\text{FWHM}(\text{UV})$ (column (7) of Table 2). The scatters is large, but it shows a weak trend for objects with $f_{esc}^{\text{Ly}\alpha} \gtrsim 0.1$, indicating that LAEs with higher $f_{esc}^{\text{Ly}\alpha}$ have *more compact* Ly α morphology.

In figure 6, we also mark out the five LyC leakers with blue squares. These LyC leakers have similar Ly α to UV continuum size ratio to the other Green Peas. We note that the other Green Peas could be unknown LyC leakers, as their current UV spectra ranges don't cover the LyC emission. The LyC leakers have 1.4 to 4.3 times larger Ly α sizes than the UV continuum sizes, so most HI gas,

which scattered Ly α emission, is unlikely to be transparent to the LyC emission. Therefore the LyC emission of these LyC leakers are probably escape through ionized holes in the interstellar medium.

6. CONCLUSION

We have investigated the Ly α and UV sizes of Green Pea galaxies using their HST-COS 2D spectra. Our main results are as follows.

1. We compared Ly α and UV sizes from the 2D spectra and 1D spatial profiles and found that most Green Peas show more extended Ly α emission than the UV continuum. We also measured the deconvolved FWHM of the spatial profiles as their Ly α and UV sizes. The Ly α sizes in most Green Peas of this sample are about 2 to 4 times larger than their UV continuum sizes. We also found the five LyC leakers in our sample have larger Ly α sizes than UV continuum sizes by 1.4 to 4.3 times.
2. In eight Green Peas, we compared the spatial profiles of Ly α photons at blueshifted and redshifted velocities, and found the blue wing of the Ly α line has a larger spatial extent than the red wing in four Green Peas with comparatively weak blue Ly α line wings.
3. Since Green Peas are analogs of high- z LAEs, our results suggest that most high- z LAEs likely have larger Ly α sizes than UV sizes. We also show that

Green Peas and MUSE $z = 3-6$ LAEs sample have similar Ly α to UV continuum size ratios.

4. We compared Ly α escape fraction with the size ratio $FWHM(Ly\alpha)/FWHM(UV)$ and found that for those Green Peas with $f_{esc}^{Ly\alpha} > 10\%$, objects with higher $f_{esc}^{Ly\alpha}$ tend to have *more compact* Ly α morphology.

The imaging and spectroscopy data are based on observations with the NASA / ESA Hubble Space Telescope, obtained at the Space Telescope Science Institute, which is operated by the Association of Universities for Research in Astronomy (AURA), Inc., under NASA contract NAS 5-26555. Some of the data presented in this paper were obtained from the Mikulski Archive for Space Telescopes (MAST). STScI is operated by the Association of Universities for Research in Astronomy, Inc., under NASA contract NAS5-26555. Support for MAST for non-HST data is provided by the NASA Office of Space Science via grant NNX09AF08G and by other grants and contracts. H.Y. acknowledges support from China Scholarship Council. H.Y. and J.X.W. thanks supports from NSFC 11421303, CAS Frontier Science Key Research Program (QYZDJ-SSW-SLH006), and the Strategic Priority Research Program “The Emergence of Cosmological Structures” of the Chinese Academy of Sciences (grant No. XDB09000000). Partial support for this work was provided by NSF grant AST-1518057.

REFERENCES

- Bond, N. A., Feldmeier, J. J., Matković, A., et al. 2010, ApJ, 716, L200
- Cardamone, C., Schawinski, K., Sarzi, M., et al. 2009, MNRAS, 399, 1191
- Charlot, S., & Fall, S. M. 1993, ApJ, 415, 580
- Dey, A., Spinrad, H., Stern, D., Graham, J. R., & Chaffee, F. H. 1998, ApJ, 498, L93
- Dijkstra, M., Haiman, Z., & Spaans, M. 2006, ApJ, 649, 14
- Dijkstra, M. 2014, PASA, 31, e040
- Feldmeier, J. J., Hagen, A., Ciardullo, R., et al. 2013, ApJ, 776, 75
- Finkelstein, S. L., Cohen, S. H., Windhorst, R. A., et al. 2011, ApJ, 735, 5
- Hayes, M., Östlin, G., Mas-Hesse, J. M., et al. 2005, A&A, 438, 71
- Hayes, M., Östlin, G., Duval, F., et al. 2014, ApJ, 782, 6
- Henry, A., Scarlata, C., Martin, C. L., & Erb, D. 2015, ApJ, 809, 19
- Hu, E. M., Cowie, L. L., & McMahon, R. G. 1998, ApJ, 502, L99
- Izotov, Y. I., Schaerer, D., Thuan, T. X., et al. 2016, MNRAS, 461, 3683
- Jaskot, A. E. & Oey, M. S. 2014, ApJ, 791, 19L
- Kashikawa, N., Shimasaku, K., Matsuda, Y., et al. 2011, ApJ, 734, 119
- Kunth, D., Leitherer, C., Mas-Hesse, J. M., Östlin, G., & Petrosian, A. 2003, ApJ, 597, 263
- Malhotra, S., & Rhoads, J. E. 2004, ApJ, 617, L5
- Mas-Hesse, J. M., Kunth, D., Tenorio-Tagle, G., et al. 2003, ApJ, 598, 858
- Matsuda, Y., Yamada, T., Hayashino, T., et al. 2012, MNRAS, 425, 878
- Matthee, J. J. A., Sobral, D., Swinbank, A. M., et al. 2014, MNRAS, 440, 2375
- Matthee, J., Sobral, D., Oteo, I., et al. 2016, MNRAS, 458, 449
- Micheva, G., Iwata, I., Inoue, A. K., et al. 2015, arXiv:1509.03996
- Møller, P., & Warren, S. J. 1998, MNRAS, 299, 661
- Momose, R., Ouchi, M., Nakajima, K., et al. 2014, MNRAS, 442, 110
- Neufeld, D. A. 1990, ApJ 350, 216
- Östlin, G., Hayes, M., Kunth, D., et al. 2009, AJ, 138, 923
- Östlin, G., Hayes, M., Duval, F., et al. 2014, ApJ, 797, 11
- Ouchi, M., Shimasaku, K., Furusawa, H., et al. 2003, ApJ, 582, 60
- Pentericci, L., Vanzella, E., Fontana, A., et al. 2014, ApJ, 793, 113
- Rauch, M., Haehnelt, M., Bunker, A., et al. 2008, ApJ, 681, 856-880
- Rhoads, J. E., Malhotra, S., Dey, A., et al. 2000, ApJ, 545, L85
- Steidel, C. C., Bogosavljević, M., Shapley, A. E., et al. 2011, ApJ, 736, 160
- Swinbank, A. M., Bower, R. G., Smith, G. P., et al. 2007, MNRAS, 376, 479
- Tilvi, V., Papovich, C., Finkelstein, S. L., et al. 2014, ApJ, 794, 5
- Treu, T., Trenti, M., Stiavelli, M., Auger, M. W., & Bradley, L. D. 2012, ApJ, 747, 27
- Verhamme, A., Schaerer, D., & Maselli, A. 2006, A&A, 460, 397
- Wisotzki, L., Bacon, R., Blaizot, J., et al. 2016, A&A, 587, A98
- Yang, H., Malhotra, S., Gronke, M., et al. 2016, ApJ, 820, 130
- Yang, H., Malhotra, S., Gronke, M., et al. 2017, arXiv:1701.01857
- Zheng, Z., Cen, R., Trac, H., & Miralda-Escudé, J. 2010, ApJ, 716, 574
- Zheng, Z.-Y., Malhotra, S., Rhoads, J. E., et al. 2016, ApJS, 226, 23